Earth and Planetary Science Letters 293 (2010) 377–387

Contents lists available at ScienceDirect

Earth and Planetary Science Letters

journal homepage: www.elsevier.com/locate/epsl

Canyon incision and knickpoint propagation recorded by apatite $^4He/^3He$ thermochronometry

Taylor F. Schildgen [a,*], Greg Balco [b,1], David L. Shuster [b,2]

[a] University of Potsdam, Institut für Geowissenschaften, Karl-Liebknecht-Str. 24-25, Haus 27, 14476 Potsdam, Germany
[b] Berkeley Geochronology Center, 2455 Ridge Road, 94709, Berkeley, CA, USA

ARTICLE INFO

Article history:
Received 10 July 2009
Received in revised form 4 December 2009
Accepted 6 March 2010
Available online 30 March 2010

Editor: T.M. Harrison

Keywords:
4He/3He thermochronometry
apatite
incision
knickpoint
uplift
Peru

ABSTRACT

In many regions of the world, deeply incised canyons demonstrate the net effects of physical processes active at Earth's surface in response to surface uplift. Low-temperature thermochronometry can constrain the timing and rates of bedrock incision, which is necessary for relating canyon incision to surface uplift over geological timescales. We analyzed four samples from the Cotahuasi–Ocoña canyon system in southwest Peru using $^4He/^3He$ thermochronometry and we present a new inversion model to identify continuous low-temperature cooling histories that are consistent with the observed data. Derived cooling histories limit the onset of fluvial incision to ~13 to 8 Ma. This is in agreement with previously reported interpretations based on a three-dimensional thermal model interpolation to a much larger set of conventional apatite (U–Th)/He ages. However, because $^4He/^3He$ thermochronometry constrains an independent cooling history for each sample, the results also permit testing of landscape-evolution models with greater spatial variability in exhumation compared to those models that can be tested by a geographically scattered set of conventional (U–Th)/He ages. The different cooling histories of the four samples require asynchronous incision along at least part of the canyon system that is best explained by headward propagation of fluvial incision by knickpoint migration.

1. Introduction

Reconstructing the evolution of surface topography through geological time can help elucidate complex relationships between tectonic forces, climate variations, chemical and physical erosion, and their resultant effects on a landscape. A common tool for this purpose is low-temperature thermochronometry. The shape of subsurface isotherms in the uppermost few kilometers of Earth's surface is perturbed by high-relief topography, so thermochronometers sensitive to cooling below ~100 °C can record past changes in the topography (e.g., Lees, 1910; Benfield, 1949; Stüwe et al., 1994; Mancktelow and Grasemann, 1997; Braun, 2002; Ehlers and Farley, 2003). A useful method to observe such changes is apatite (U–Th)/He thermochronometry. As an apatite grain approaches the surface, it begins to retain radiogenic ^4He below ~85 °C (e.g., Farley, 2000; Reiners and Farley, 2001; Flowers et al., 2009), which corresponds to ~1.5–2 km depth, depending on the cooling rate and the local geothermal gradient. Although complete retention of ^4He (i.e., He closure) does not occur instantaneously, conventional (U–Th)/He chronometry yields a unique closure age from the total ^4He abundance in an apatite grain. Thus, inferring a landscape-scale cooling history requires (U–Th)/He ages of geographically distributed samples that cooled at different times, and a quantitative thermal model that relates the cooling histories at the sample sites to one another. Typically, a model predicts ages based on a prescribed exhumation history, and comparison against the measured ages can identify a set of best-fitting exhumation histories. This approach has been used to address a number of questions in landscape evolution, including the evolution of orogenic relief (Braun and Robert, 2005; Herman et al., 2007), tectonics and exhumation of the Himalayan front (Huntington et al., 2007; Whipp et al., 2007), and the timing of canyon incision (Clark et al., 2005; Schildgen et al., 2007).

Apatite $^4He/^3He$ thermochronometry provides a different approach (Shuster and Farley, 2004; Shuster et al., 2005; Shuster and Farley, 2005). This method determines the spatial distribution of ^4He within an apatite grain, which is a function of cooling history near and below the He closure temperature. In contrast to conventional (U–Th)/He thermochronometry, in which a cooling history can only be obtained from multiple samples linked by model assumptions, $^4He/^3He$ thermochronometric data from a single sample independently constrains its continuous low-temperature cooling history. This method reduces the number of geographically distinct samples required to infer a landscape-scale cooling history, and provides

* Corresponding author. Tel.: +49 331 977 5849; fax: +49 331 977 5700.
E-mail addresses: tschild@uni-potsdam.de (T.F. Schildgen), balcs@bgc.org (G. Balco), shuster@bgc.org (D.L. Shuster).
[1] Tel.: +1 510 644 1341; fax: +1 510 644 9201.
[2] Tel.: +1 510 644 9891; fax: +1 510 644 9201.

0012-821X/$ – see front matter © 2010 Elsevier B.V. All rights reserved.
doi:10.1016/j.epsl.2010.03.009

increased resolving power at temperatures near and below the closure temperature.

We applied $^{4}He/^{3}He$ thermochronometry to four apatite samples from Cotahuasi–Ocoña canyon in southwest Peru. The thermal history of this canyon system has already been interrogated by a set (24 samples) of conventional (U–Th)/He ages interpreted with a 3-d thermal model (Schildgen et al., 2009a). Here, we describe a new inversion scheme for identifying thermal histories from $^{4}He/^{3}He$ analysis and show that the $^{4}He/^{3}He$ results from only a few samples reproduce the thermal history obtained from the much larger (U–Th)/He data set without recourse to spatial interpolation of cooling age information between sample locations. Finally, we compare the

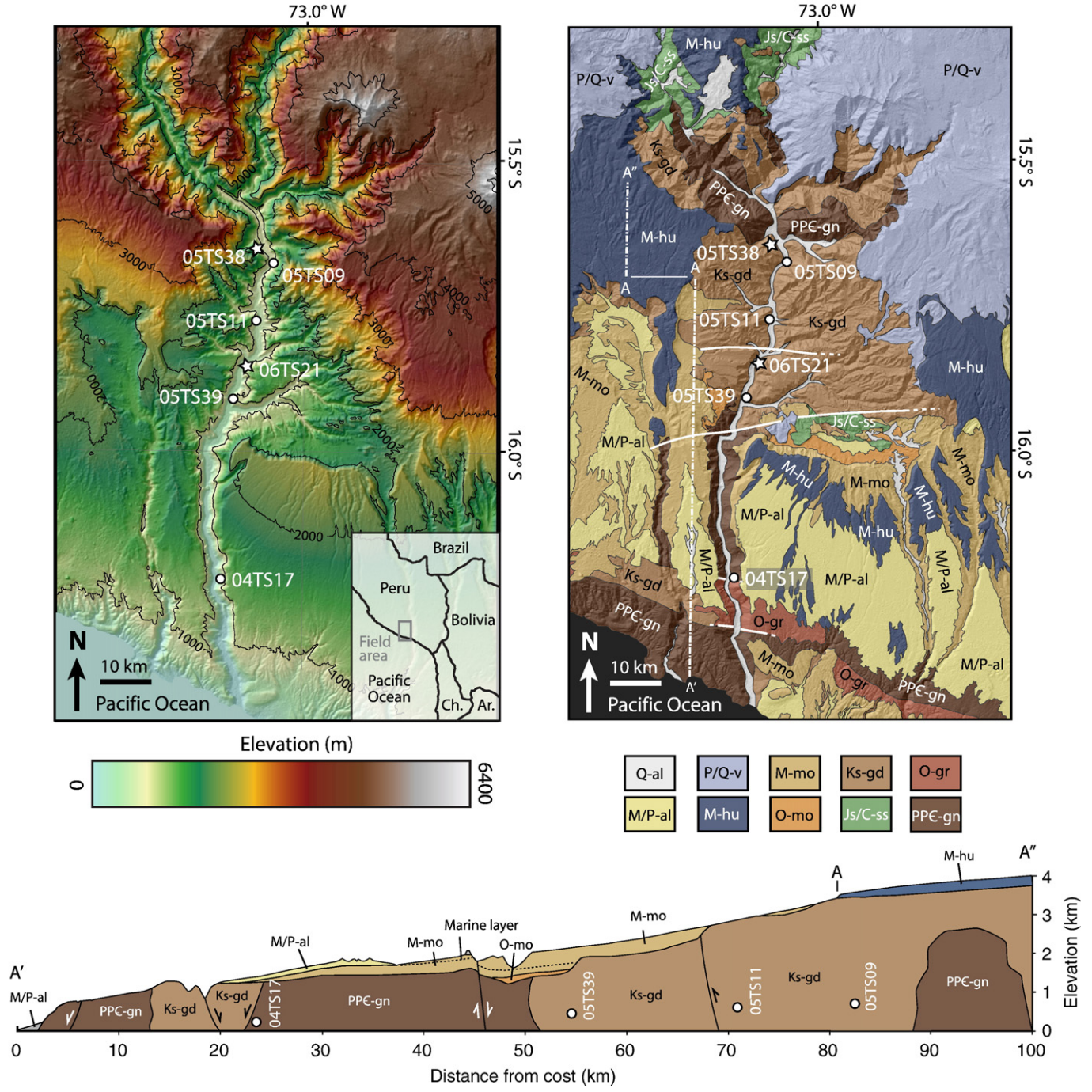

Fig. 1. Sample locations and geologic context. Panel on left shows samples analyzed for $^{4}He/^{3}He$ thermochronology (white circles) and $^{40}Ar/^{39}Ar$ dated volcanic flows (white stars; from Schildgen et al., 2007; 2009a) on a 30-m resolution digital elevation model derived from Advanced Spaceborne Thermal Emission and Reflectance Radiometer (ASTER) imagery. Contour interval is 1000 m. Volcanic flows beneath white stars are too small to appear on the scale of the map. Panel on right shows ASTER-derived shaded relief overlain by geologic data based on Schildgen et al. (2009b) and Instituto Geológico Minero y Metalúrgico (INGEMMET) (2001). Faults (white lines) are based on mapping by Roperch et al. (2006) and Schildgen et al. (2009b). Symbols on map and on cross-section beneath map include Q-al: Quaternary alluvium; M/P-al: Mio-Pliocene alluvium/landslide; P/Q-v: Plio-Quaternary volcanics; M-hu: Miocene Huaylillas ignimbrite; M-mo: Miocene upper Moquegua Group sediments; O-mo: Oligocene lower Moquegua Group sediments; Ks-gd: Cretaceous granodiorite, diorite, and tonalite; Js/C-ss: Jurassic/Cretaceous sandstone and carbonate; O-gr: Ordovician granites; and PPC-gn: Precambrian gneiss. Geologic cross-section spans the region from A″ to A and from A to A′, as shown by the dashed-dotted line on the geologic map. Vertical exaggeration in the cross-section is 3:1, with the locations of samples interpolated from their positions within the canyon.

^{4}He/^{3}He inversion results with thermal model predictions to argue that the ^{4}He/^{3}He results record the progress of headward-propagating canyon incision by knickpoint migration.

2. The Cotahuasi–Ocoña canyon system

Topography in southwest Peru rises from a 1-km-high coastal escarpment up to nearly 5 km elevation across a broad, low-relief surface, which is incised by Cotahuasi–Ocoña canyon (Fig. 1). The region is underlain by Precambrian through Cretaceous basement rocks capped by the ~50–16 Ma Moquequa Group clastic sediments, the 14–16 Ma Huaylillas ignimbrite, Mio-Pliocene gravels, and younger volcanics. Although the Moquegua Group sediments record the presence of significant topography before 14 Ma (e.g., Sempere et al., 2004; Roperch et al., 2006), additional surface uplift on the order of 2.4–3.0 km occurred between ~14 and 2.2 Ma (Schildgen et al., 2009b) through crustal-scale monocline deformation (e.g., Isacks, 1988; Wörner et al., 2002; Schildgen et al., 2009b), minor normal faulting, and block uplift (Schildgen et al., 2009b). Base level changes may contribute complexity to the landscape-evolution history, however, sea level has dropped by only ~40 m since the early Oligocene with shorter-term variations of ~20–80 m (Miller et al., 2005), implying that it is insignificant compared to late Cenozoic surface uplift in southwest Peru.

Because incision of the canyon system must coincide with or postdate surface uplift, we should be able to determine the timing of surface uplift by i) dating the onset of incision, and ii) estimating the lag time between uplift and incision. This includes determining whether canyon incision was spatially uniform, or proceeded by headward propagation of a major knickpoint formed at the coast (Fig. 2). Knickpoints commonly develop along rivers that incise in response to climate change, base level change, and/or tectonic forcing (e.g., Seeber and Gornitz, 1983; Rosenbloom and Anderson, 1994; Seidl et al., 1994, 1996; Whipple and Tucker, 1999; Snyder et al., 2000; Kirby and Whipple, 2001; Wobus et al., 2003, 2006; Zaprowski et al., 2005), and separate the downstream "adjusted" regions of a river from upstream "unadjusted" regions. If a major knickpoint did form in response to surface uplift in southwest Peru, what was the rate of knickpoint headward propagation? Answering this question would provide a better framework for relating fluvial incision to surface uplift, which in turn would allow for improved estimates for the timing of uplift in southwest Peru.

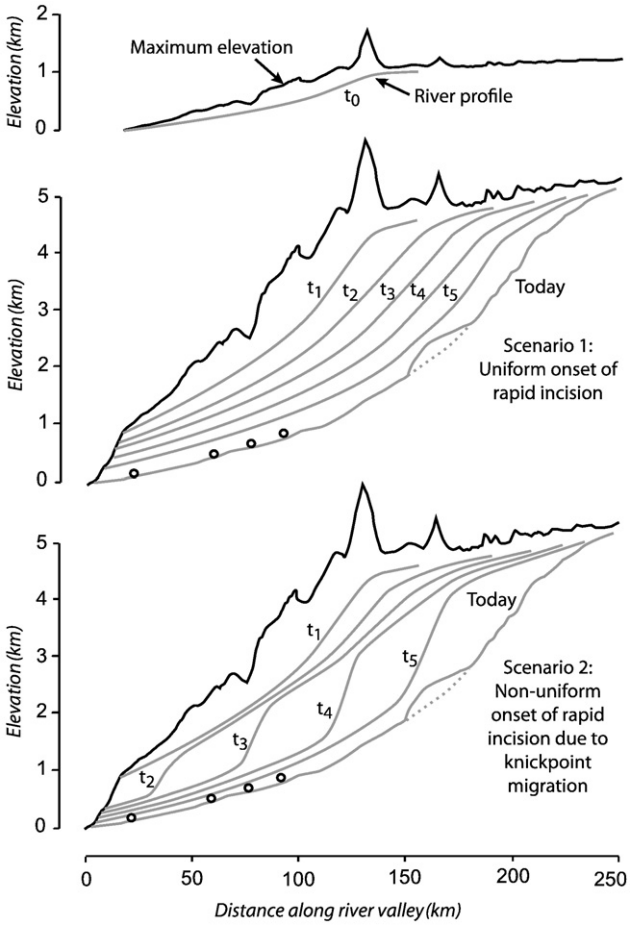

Fig. 2. Schematic, hypothetical end-member scenarios of canyon incision following surface uplift of the western margin of the Andean plateau. Top profile is a schematic illustration of surface topography (black lines) and the river profile (gray line) prior to late Cenozoic surface uplift. Middle and bottom profiles are schematic illustrations of two end-member scenarios for evolution of the river profile through five time steps (t_1–t_5), ending with the modern river profile ("Today"). The dashed line along the modern river profile illustrates what we assume is the top of bedrock (discussed in Section 6.4). Black line in the middle and bottom profiles shows modern topography. White circles show sample locations.

3. Previous constraints on river incision history and surface uplift

Dating surface uplift by dating river incision requires two pieces of information: the timing of incision, and the lag time between uplift and incision. Schildgen et al. (2007) argued that in the Cotahuasi–Ocoña system, the lag time should be short given the size of the drainage system and high discharge. This should lead to rapid propagation of knickpoints through the drainage system and similarly rapid fluvial response time (e.g., Whipple and Tucker, 1999; 2002). Although several lines of evidence suggest long-term stability of the hyper- to semi-arid climate in the region (e.g., Alpers and Brimhall, 1988; Sillitoe and McKee, 1996; Rech et al., 2006), drying of the western margin likely occurred in response to the growth of the Central Andean orographic rain shadow (e.g., Lenters and Cook, 1995; 1997; Houston and Hartley, 2003; Strecker et al., 2007; Bookhagen and Strecker, 2008; Ehlers and Poulsen, 2009). Nonetheless, large areas of the regional surface in the forearc region that remain undissected (marked by the Huaylillas ignimbrite and its overlying alluvial cover in Fig. 1) highlight the potential for large geographic variations in lag time. This was demonstrated by Hoke et al. (2007), whose longitudinal profiles of rivers throughout the western margin of northern Chile showed wide variations in the position of knickpoints and in the inferred lag time of the different systems. In general, larger catchments that tap into high elevation regions with their accompanying higher precipitation have shorter potential lag times, but details of this have not yet been examined.

Existing information on the timing of Cotahuasi–Ocoña canyon incision includes radiometric ages of infilling volcanic flows (Thouret et al., 2007; Schildgen et al., 2007, 2009a,b) and apatite (U–Th)/He data from Schildgen et al. (2007, 2009a). Thouret et al. (2007) showed that an ignimbrite inset below the regional surface records incision initiation before 9 Ma, and that volcanic flows at low elevations in the upper portion of the catchment indicate that incision was nearly complete by 3.8 Ma. Schildgen et al. (2007) showed that conventional apatite (U–Th)/He ages revealed a strong contrast between old ages (~9–60 Ma) associated with slow erosion of the upland surface and much younger ages within the canyon (~5–9 Ma), suggesting an increase in the cooling rate and hence canyon incision starting at ~9 Ma. Because this relationship could also in part reflect lateral variability in the crustal thermal structure, Schildgen et al. (2009a) used a three-dimensional, time-dependent thermal model (using a modified version of Pecube; Braun (2005) and references within) to distinguish the spatial and temporal changes in the crustal thermal structure. The model was forced by a prescribed landscape-evolution history in which slow regional exhumation was followed by rapid incision along the entire length of the canyon. Their results supported

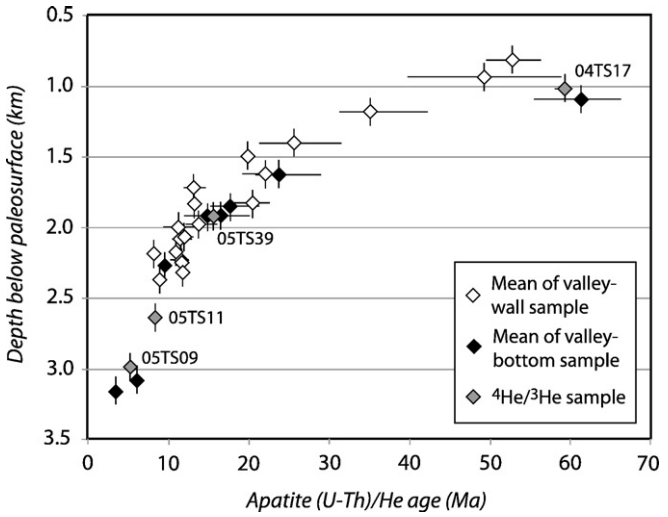

Fig. 3. Conventional apatite (U–Th)/He data published by Schildgen et al. (2007) and Schildgen et al. (2009a), highlighting the context of samples analyzed here for $^4He/^3He$ thermochronometry. Large symbols represent the mean age for each sample. Horizontal error bars represent the range of individual crystal ages for each sample, and vertical error bars represented the estimated error on the calculated depth below the paleosurface. Samples are plotted versus depth beneath the regional paleosurface to correct for the long-wavelength topographic effects on sampling along the valley bottom (e.g., Clark et al., 2005; Huntington et al., 2007).

the hypothesis that canyon incision began ~9 Ma: only model runs in which incision started at 8–11 Ma yielded acceptable fits to the (U–Th)/He data set (Schildgen et al., 2009a).

The purpose of this study is to directly test this result by applying $^4He/^3He$ thermochronometry at four sites along the canyon floor. Our objective is to independently determine the onset time and the rate of rapid cooling associated with canyon incision at all four sites without linking geographically dispersed closure ages with a thermal model. In turn, two models can be tested using the $^4He/^3He$ thermochronometric data: Was canyon incision spatially uniform along the canyon longitudinal profile, or did it proceed by slow headward knickpoint propagation? If the latter, how may the knickpoint propagation rate affect estimates for the start of incision and constraints on surface uplift?

4. Analytical methods

We analyzed four samples along a valley-bottom transect of Ocoña canyon, ranging from 27.7 to 80.1 km inland from the coast (Fig. 1). Apatite (U–Th)/He ages of the selected samples (determined using conventional methods and originally reported in Schildgen et al., 2007) range from ~58 to ~5 Ma (Fig. 3), spanning nearly the full range of apatite (U–Th)/He ages reported for the region. Additional apatites from the same rock samples were exposed to $\sim 4.6 \times 10^{15}$ protons/cm^2 with incident energy ~220 MeV over a continuous 8 hour period at The Francis H. Burr Proton Therapy Center (Shuster et al., 2004). From each irradiated sample, we selected euhedral apatite grains with pristine crystal faces and analyzed aliquots of between 1 and 3 grains. The crystals were sequentially heated in multiple steps under ultra-high vacuum while in contact with a type-C thermocouple using a feedback-controlled diode laser. The ^3He abundance and the $^4He/^3He$ ratio were measured for each heating step using conventional sector-field mass spectrometry and corrected for blank contributions to ^3He and ^4He (Table S1). Ratio uncertainties shown in Fig. 4 and reported in Table S1 contain propagated uncertainty in blank corrections.

5. Forward model and random-search inversion scheme

We developed a numerical model that predicts the (U–Th)/He age and the evolution of the $^4He/^3He$ ratio during a step-degassing experiment (i.e., $^4He/^3He$ ratios versus the cumulative ^3He release fraction, ΣF^3He), and whose input parameters are the characteristics of the analyzed crystal(s) and a cooling history. We then used a random-search scheme modeled on that of Ketcham (2005) to find cooling histories that were compatible with the observations. This model framework has four components: i) a scheme to generate random time–temperature (t–T) histories; ii) a forward model whose input is a t–T history and that predicts the total abundance and radial distribution of ^4He in the sample (henceforth, the 'geologic model'); iii) a forward model whose input is the ^4He distribution in the sample and that predicts the $^4He/^3He$ ratios evolved during the step-degassing experiment (the 'degassing model'); and iv) a means of determining whether the model results fit the observations.

5.1. Time–temperature (t–T) histories

To generate trial cooling histories, the model first generates a sequence of temperatures with an autoregressive model $T(i) = T(i-1) - e(i)$, where $T(i)$ is the temperature in step i (arbitrary units), $T(0) = 0$, $e(i)$ is normally distributed random with mean k and standard deviation 1, and values of $e(i) < 0$ are set to 0. This scheme enforces a monotonic cooling history with no reheating (which is justified by a lack of any volcanic flows in the proximity of bedrock sample locations), but permits long periods at constant temperature. We paired these temperatures with a corresponding sequence of times chosen from a uniform distribution between 0 and 1, then shifted and scaled both sequences to geologically appropriate values. All cooling histories began at 150 °C at a time older than twice the measured (U–Th)/He age of the sample, and ended at the modern mean surface temperature of the sample site. We chose the parameter k, as well as the number of t–T points, to populate the t–T space as fully as possible; the number of t–T points was allowed to vary randomly between 6 and 10.

5.2. Geologic and degassing models

The geologic model for ^4He accumulation during cooling uses the Crank–Nicholson finite-difference scheme for diffusion in a sphere described by Ketcham (2005). The scheme for alpha particle ejection and redistribution is also described in that reference; in this study we assumed a uniform distribution of U and Th. Apatite diffusion kinetics is described by the radiation damage and annealing model (RDAAM) of Flowers et al. (2009). This model differs from previous models for the effect of radiation damage on apatite diffusion kinetics (Shuster et al., 2006) in that the effective annealing temperature for radiation damage (~100 °C) is well above the He closure temperature (~70 °C). This affects predictions for the (U–Th)/He age of samples that experience long residence near, or slow cooling through, the He partial retention zone (PRZ) (also see discussion below).

Fig. 4. $^4He/^3He$ ratio evolution diagrams for step-heating experiments (a–d) and associated cooling paths (e–h). Plots on left show the $^4He/^3He$ measurements of each step (R_{step}) normalized to the bulk ratio (R_{bulk}) determined by integrating all steps (black circles; the vertical axes of open boxes indicating 1 standard error) plotted against the cumulative ^3He release fraction (ΣF^3He). Green, yellow, and orange lines show modeled cooling paths. Green lines are cooling paths that show a good fit to the data, while yellow and orange lines show progressively worse fits that can be excluded at a 99% confidence level based on our statistical assessment (see text for discussion). Plots on right show the green, yellow, and orange modeled cooling paths in time–temperature space; gray paths indicate modeled cooling paths that failed to predict the observed (U–Th)/He age.

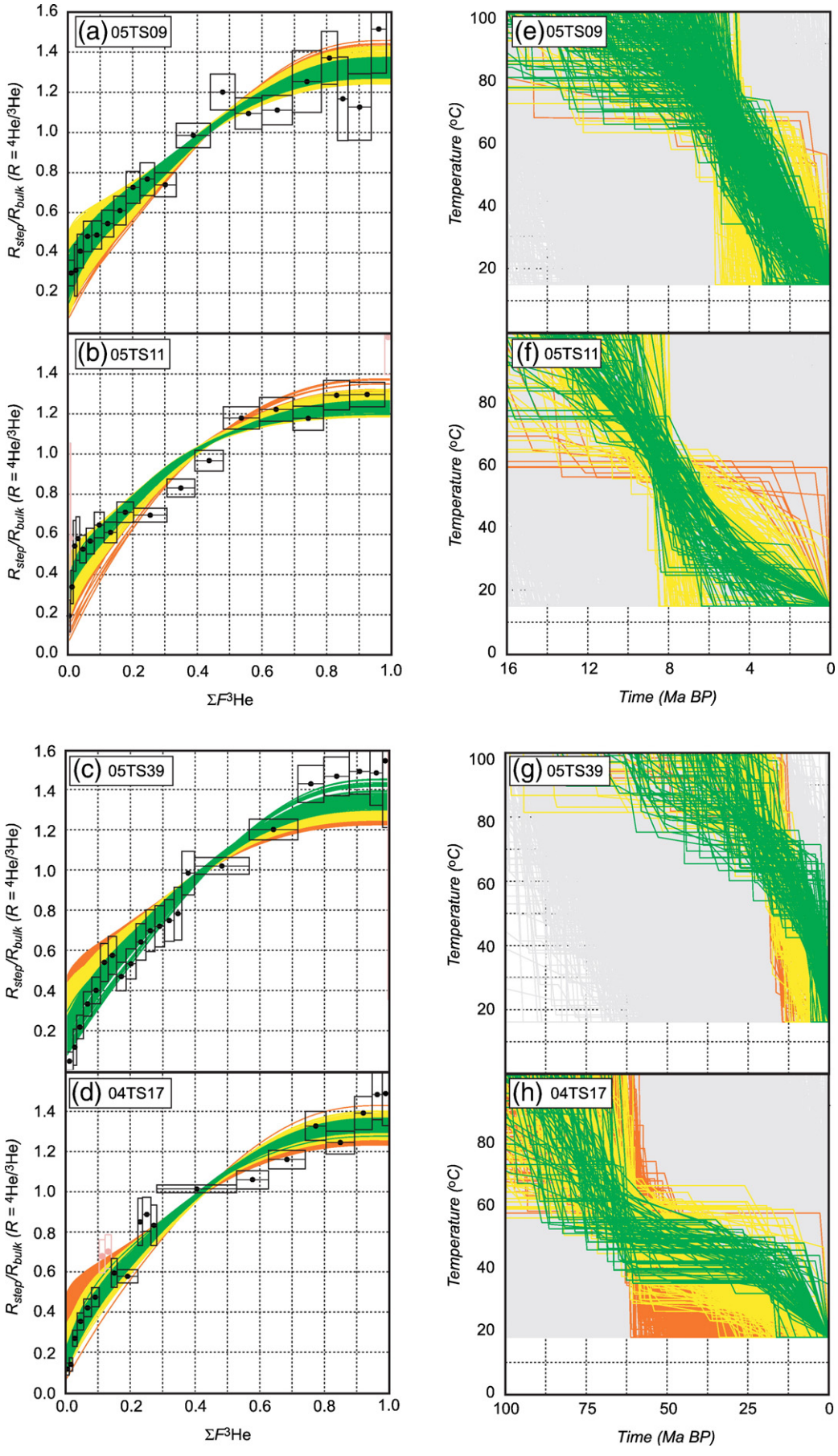

The degassing model employs the same finite-difference scheme. The initial condition for the radial ^{4}He distribution is taken from the end state of the geologic model, and ^{3}He is initially uniformly distributed throughout the grain. As we are predicting the normalized ^{4}He/^{3}He ratio, the value chosen for the He diffusivity in this portion of the model does not affect the results; only the relationship between ^{3}He and ^{4}He diffusivities is important. Following Shuster et al. (2004) we take the diffusivities of ^{3}He and ^{4}He to be equal.

5.3. Model fitting

To determine whether or not a trial cooling history fits the observations, we need to answer two questions. First, does it predict the correct (U–Th)/He age? Second, does the predicted ^{4}He/^{3}He ratio evolution agree with that observed? Although one could construct a fit statistic that included both of these tests, we considered each separately. First, we ran the geologic model for all trial cooling histories, and rejected those that did not predict a (U–Th)/He age within 1 standard error of the measured age. Second, for those cooling histories that passed this screening, we ran the degassing model, compared the resulting predicted ^{4}He/^{3}He ratio evolution to the ratios actually observed, and assigned a misfit value based on this comparison.

We used a misfit statistic M defined to be the mean of squared residuals weighted by the mean uncertainty in the ratio measurements:

$$M = \frac{1}{n}\sum_{i=1}^{n}\left(\frac{R_{p,i}-R_{m,i}}{\bar{\sigma}}\right)^2 \quad (1)$$

where $R_{p,i}$ is the predicted normalized ^{4}He/^{3}He ratio released in heating step i, $R_{m,i}$ is the measured value, n is the number of heating steps, and $\bar{\sigma}$ is the mean ratio measurement uncertainty in the experiment. For a typical number of heating steps ($n=20$), the expected value of this statistic (estimated by a Monte Carlo simulation) is ~0.95. That is, if the actual ^{4}He/^{3}He ratios were in fact as predicted by the model, and our estimate of the measurement precision is correct, M would exceed this value 50% of the time. The corresponding 99% confidence level for M is ~2. According to this argument, we defined thermal histories yielding $M<2$ to be acceptable fits to the data.

This argument, however, has several weaknesses. First, it assumes that the model perfectly describes the evolution of He distributions in the sample during both its geologic history and the degassing experiment. This is not actually the case, because we have not included a variety of complicating factors in the geologic and degassing models, including zonation in [U] and [Th], the non-spherical shape of apatite crystals, and small differences in size, shape, and diffusion kinetics between grains analyzed together in the degassing experiment. Although in all cases we obtained good fits to the data without including these factors, we cannot exclude the possibility that they affect the results. Second, this fit statistic does not detect the presence of systematic residuals. Fig. 4 shows that many predicted ^{4}He/^{3}He evolutions yielding acceptable values for M show systematic differences from the observations. This could signal an incorrect cooling history, but could also arise solely from the model simplifications listed above. Third, our choice of this fit statistic avoids the issue of degrees of freedom that is implicit in evaluating other commonly used fit statistics such as the reduced chi-squared or the MSWD. Although in principle one could estimate degrees of freedom for this purpose on the basis that the number of input parameters in the model is twice the number of randomly generated t–T points in the cooling history, this would be misleading because the portions of the cooling history that are well above or below the He PRZ have no effect on the result.

6. Results and discussion

6.1. t–T paths derived from ^{4}He/^{3}He inversion

Fig. 4 shows results of the random-search inversion models for the four samples. Of the large set of possible cooling paths that yield the observed total (U–Th)/He age for a given sample (colored paths), only a small subset also yield acceptable fits to the ^{4}He/^{3}He measurements (green paths). These results highlight the advantage of ^{4}He/^{3}He thermochronometry over conventional (U–Th)/He dating for identifying the cooling history near the He PRZ. Cooling histories are unconstrained for temperatures above the He PRZ and are tightly constrained as the sample cools below the closure temperature (see discussion in Shuster and Farley, 2004). The set of acceptable cooling histories can be reduced by incorporating additional geologic information: using ^{40}Ar/^{39}Ar geochronometry, Schildgen et al. (2007, 2009a) dated two volcanic flows ≤100 m above of the current valley floor in the central canyon region to 2.2 and 2.3 Ma. This requires that incision, and hence cooling of canyon-bottom samples to surface temperature, must have been complete by that time and allows us to exclude otherwise acceptable cooling paths that do not satisfy this condition (Fig. 5).

^{4}He/^{3}He results from two downstream samples require a marked increase in cooling rate, presumably induced by rapid canyon incision. Sample 04TS17, 27.7 km inland from the coast, cooled slowly through and below the He PRZ, and then cooled rapidly from ~40 °C to surface temperature (Fig. 5(b)). Cooling histories that fit the ^{4}He/^{3}He results from this sample display a tradeoff between the cooling rate in the He PRZ and the time rapid cooling begins: the slower the early cooling, the later the onset of rapid cooling. Because of this tradeoff, the time that rapid cooling began is only limited to be between 25 and 3 Ma. Sample 04TS39, 52.8 km inland, did not reside in the He PRZ for as long, but nearly all acceptable cooling histories require an equivalent increase in the cooling rate at some time between 13 and 3 Ma (Fig. 5(a)). For nearly all acceptable cooling paths for both of these samples, rapid cooling is sustained until 3–2.2 Ma (Fig. 5).

The two upstream samples do not record the increase in cooling rate required by the two downstream samples. Rapid cooling was already in progress at the time they began to retain ^{4}He, implying that they were beneath the He PRZ at the onset of rapid cooling (they are located 2640 and 2990 m below the regional surface) (Fig. 5(c,d)). The ^{4}He/^{3}He results from the upstream samples therefore provide minimum ages for the onset of rapid cooling, the time these samples cooled to surface temperatures, and cooling rates during the latter stages of cooling. Due to the shorter overall time period recorded by these samples, they provide better resolution on the latter stages of the cooling history than the downstream samples. At sample 05TS11, 68.7 km inland from the coast, rapid cooling started before 8 Ma and ended 6–2.2 Ma (Fig. 5(d)). Nearly all acceptable cooling paths at this site display a decreasing cooling rate towards the present. At sample 05TS09, 80.1 km inland, rapid cooling started before ~6 Ma and ended 3–2.2 Ma (Fig. 4(c)). Most acceptable cooling paths for this sample show an approximately constant cooling rate sustained until 2.2 Ma.

To summarize, the ^{4}He/^{3}He results show that: i) there was a change from slow cooling consistent with slow background erosion rates to rapid cooling consistent with canyon incision; ii) the onset of rapid cooling occurred 25–3 Ma near the coast and prior to 8–6 Ma inland, and iii) rapid cooling was sustained until 6–2.2 Ma and 3–2.2 Ma at the two upstream sample sites.

6.2. Cooling histories inferred from ^{4}He/^{3}He data compared to those from conventional apatite (U–Th)/He ages and thermal model interpolation

As discussed above, Schildgen et al. (2009a) used a time-dependent thermal model driven by an assumed incision history to

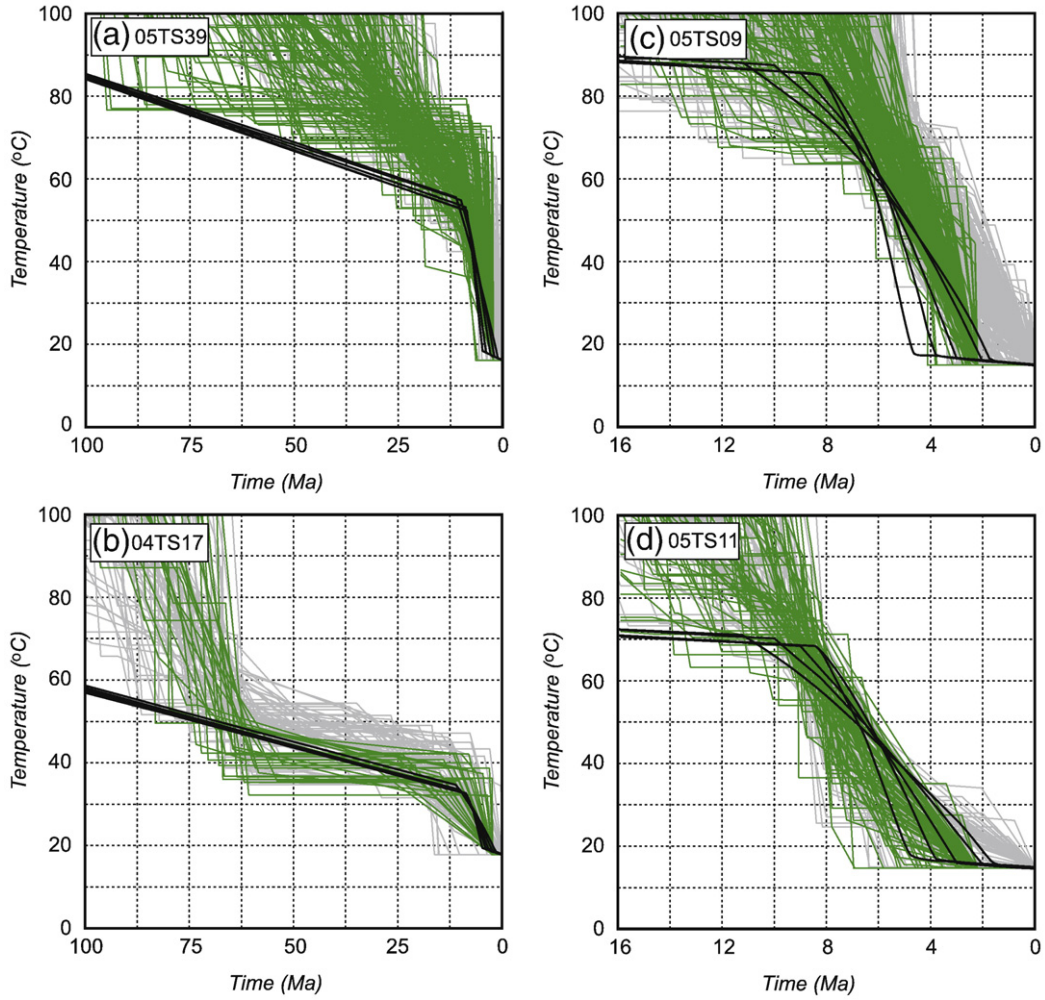

Fig. 5. Cooling paths constrained by ^{4}He/^{3}He data (gray and green lines) and from Pecube simulations optimized to predict conventional apatite (U–Th)/He ages of 24 different samples (black lines). Both sets of cooling histories represent the full range of acceptable *t–T* paths derived from the different data sets. Gray lines show paths that fit the ^{4}He/^{3}He data but do not fit the geological constraint of no cooling after 2.2 Ma based on the dated volcanic flow at the present valley bottom (Schildgen et al., 2009a). Note change in *x*-scale between panels a and b (100 to 0 Ma) and panels c and d (16 to 0 Ma).

identify incision and cooling histories that were consistent with their conventional (U–Th)/He measurements. They compared the model-predicted ages to the measured ages to assess the adequacy of a given model. Acceptable parameter values (i.e., those that predicted (U–Th)/He ages indistinguishable from measured ages at a 95% confidence level derived from a chi-square misfit statistic) include incision onset times ranging from 8 to 11 Ma and completion times ranging from 2 to 5 Ma. These constraints on the timing of incision are reflected as breaks in slope of the *t–T* paths derived from Pecube (Fig. 5).

At temperatures within and below the He PRZ, acceptable cooling paths derived from our ^{4}He/^{3}He inversion are in good agreement with the thermal-model-derived cooling paths that Schildgen et al. (2009a) found to yield acceptable fits to the conventional (U–Th)/He age data set (Fig. 5). Differences between the acceptable cooling paths derived from the different methods exist at higher temperatures. For example, at sample 04TS39, the cooling history prior to incision derived from the thermal model fit to the entire (U–Th)/He data set indicates lower temperatures before 25 Ma than permitted by the ^{4}He/^{3}He results for this sample. These differences arise for two reasons. First, the acceptable cooling histories derived from the thermal modeling of Schildgen et al. (2009a) are chosen to yield an acceptable fit to the (U–Th)/He data set as a whole, but not necessarily to any single (U–Th)/He age. Second, and more importantly, our ^{4}He/^{3}He inversion model employs a time-dependent annealing model for He diffusion kinetics (Flowers et al., 2009), whereas Schildgen et al. (2009a) computed (U–Th)/He ages from model-derived cooling histories using constant Durango apatite diffusion kinetics (Farley, 2000). This difference in diffusion kinetics significantly affects age predictions for samples that experience a long residence in the He PRZ. In the model framework of Schildgen et al. (2009a), the older (U–Th)/He ages that are affected by this difference in diffusion kinetics help to identify the background erosion rate prior to canyon formation. The younger ages that provide strong constraints on the timing of canyon formation, on the other hand, did not experience long residence in the He PRZ, so are not strongly affected. To summarize, if Schildgen et al. (2009a) had used the time-dependent model for He diffusion kinetics, they would have inferred a different background erosion rate, but the same beginning and ending times for canyon incision. In this study we are primarily interested in dating the rapid cooling associated with canyon incision, so we have not considered this issue further.

6.3. Advantages of ^{4}He/^{3}He data thermochronometry for incision and landscape-evolution studies

Overall, the agreement between cooling histories derived from four ^{4}He/^{3}He analyses and those derived from thermal model

interpolation to a large set of conventional (U–Th)/He ages highlights several advantages of $^4He/^3He$ thermochronometry. First, a relatively small number of analyzed samples can provide information on regional cooling histories. In this case we obtained comparable constraints on the incision history of Ocoña canyon from four samples as did Schildgen et al. (2009a) from 24 samples. This highlights the utility of $^4He/^3He$ thermochronometry in areas where access to sampling localities may be highly limited (e.g., Colgan et al., 2008).

In addition, we found that the $^4He/^3He$ data for samples from relatively shallow depths provide information on canyon incision. This is particularly evident near the coast, where samples only ~1 and 2 km beneath the regional paleosurface (04TS17 and 05TS39) clearly require a significant recent change in the cooling rate. In contrast, a valley-wall transect of conventional (U–Th)/He ages from the canyon rim to bottom at these sites would not extend below the He PRZ at the time incision started, so could only provide information about the early, relatively slow cooling history prior to incision. This demonstrates that $^4He/^3He$ thermochronometry can be useful for interrogating landscape evolution in areas where sampling access is limited and total exhumation or relief change is less than the depth to the He PRZ.

Finally, cooling histories derived from $^4He/^3He$ data are independent of assumptions in typical thermal models that are required to link multiple, spatially scattered (U–Th)/He ages into a continuous cooling history. This is important because it improves our ability to learn about spatial patterns of exhumation. A limitation of the previous conventional (U–Th)/He work is that the majority of samples were collected from the canyon bottom, and it was only possible to collect valley-wall transects of samples at locations near the middle of the canyon. Thus, the lateral position of the samples is strongly correlated with sample depth below the pre-incision surface. Such correlation makes it difficult to test whether canyon incision proceeded simultaneously at all locations, or if incision began at the coast and propagated headward along the longitudinal profile. Because the $^4He/^3He$ data independently constrain cooling histories at multiple locations, we can test these two hypotheses in following section despite a lack of valley-wall sample transects.

6.4. Uniform incision or knickpoint migration?

A primary motivation of this study was to learn about canyon incision processes in response to surface uplift by testing whether the onset of incision was contemporaneous throughout the canyon system or propagated headward from the coast through knickpoint migration (Fig. 2). The former may occur if the river is uniformly steepened, such as through deformation of the western Andean margin into a crustal-scale monocline (e.g., Isacks, 1988; Wörner et al., 2002; Schildgen et al., 2009b). With current analytical techniques, it may not be possible to resolve truly uniform onset of incision from fast migration of a major knickpoint, or from the migration of a series of small knickpoints that develop during surface uplift. Regardless, these scenarios producing uniform or nearly-uniform onset of incision would imply a short lag time between the onset of surface uplift and the onset of canyon incision measured at any point, meaning that incision tightly limits the onset of surface uplift. Slow migration of a major knickpoint, however, would require estimates of the propagation rate to effectively limit the onset of surface uplift. The simplest way to distinguish uniform onset of incision from slow knickpoint propagation would be to resolve differences in the onset of incision-induced rapid cooling along the longitudinal profile; uniform incision would induce simultaneous cooling, and slow knickpoint propagation would induce time-transgressive cooling that proceeds upward from the coast.

Unfortunately, the conventional (U–Th)/He ages and our $^4He/^3He$ data results do not constrain incision onset times with sufficient precision to distinguish the two hypotheses. This is mainly because the samples with the youngest (U–Th)/He ages, where we would expect to best resolve the recent cooling history, were located below the He PRZ at the time canyon incision began, so do not record this event. The downstream samples, as discussed above, require accelerated cooling but do not precisely date its initiation. We can conclude only that rapid cooling began 25–3 Ma at 04TS17, 13–3 Ma at 04TS39, >8 Ma at 04TS11, and >6 Ma at 04TS09. These results are consistent with either simultaneous or headward-propagating incision models, the extreme possibilities being simultaneous incision beginning 13–8 Ma, or headward-propagating incision beginning 25–13 Ma at the coast and 6 Ma at our farthest upstream sample. The $^4He/^3He$ inversion model results for all sites are in agreement with a scenario in which rapid incision was sustained until 3–2.2 Ma. However, scenarios in which cooling ended later at samples farther upstream are permitted.

An alternative test for the simultaneous onset of incision is to compare the $^4He/^3He$ inversion model results of the two upstream samples, 05TS11 and 05TS09. These samples have the youngest (U–Th)/He ages and therefore provide highest resolution on recent cooling. They clearly do not share a common cooling history (Fig. 6). For example, at 6 Ma, 05TS09 is at least 20 ° C warmer, and cooling faster, than 05TS11. This suggests a temporal offset in cooling at these two sample locations, with a sense consistent with headward knickpoint propagation: cooling likely started earlier at the downstream sample, 05TS11. However, this could potentially also be explained by the difference in the samples' depth below the pre-incision surface: 05TS09 is 350 m deeper than 05TS11. We evaluated this possibility by comparing the $^4He/^3He$ based inversion results of these samples with the cooling histories derived from selected thermal model simulations in Schildgen et al. (2009a). Those model simulations assumed that incision was simultaneous at both sites, and took into account the different depths beneath the pre-incision surface by tracking of the samples' complete exhumation and cooling history. The models therefore provide limits on what cooling history differences should be expected between these two sample sites given simultaneous onset of incision. Nearly all acceptable cooling histories derived from $^4He/^3He$ data of these two samples imply a larger temperature difference prior to ~4 Ma than is permitted by the

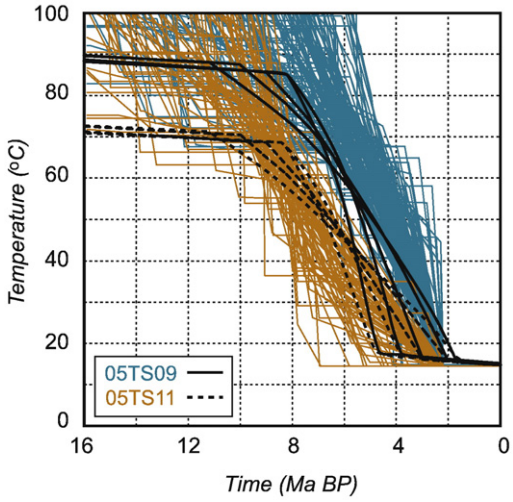

Fig. 6. Stacked cooling paths derived from Pecube 3-d thermal model (black lines) and from $^4He/^3He$ inversions (colored lines) for samples 05TS09 and 05TS11. The Pecube thermal model simulations assume simultaneous canyon incision at both sites, but a range of starting and ending times.

simultaneous-onset incision model (Fig. 6; note differences between the black and colored cooling paths). This suggests that incision at 05TS11 preceded incision at 05TS09 by 1 to 2 Ma, and supports a scenario in which canyon incision, at least between samples 05TS11 and 05TS09, proceeded by headward propagation of a knickpoint over ~12 km at an apparent rate of 6 to 12 km/Ma.

If the ~6 to 12 km/Ma knickpoint propagation rate is characteristic of the whole canyon, it would imply that incision at the coast started ~7 to 13 Ma earlier than at sample 05TS09. However, this interpretation of the data would imply that there should be a major knickpoint farther upstream along the >250 km length of the Cotahuasi–Ocoña river system, above which no significant incision should have occurred. Although there is a broad convexity in the river profile between 1.8 and 2.8 km elevation (~175 to 220 km upstream from the coast) (Fig. 7), it does not appear to be a major bedrock knickpoint. Thouret et al. (2007) argued that the canyon in that region was mostly incised by 3.8 Ma (based on a $^{40}Ar/^{39}Ar$ dated valley-filling ignimbrite), was then refilled by 2-Ma ignimbrites that blanket the plateau in the region, and subsequently has been re-incised. The re-incised portion was then partially refilled by extensive landsliding of the weakly welded 2-Ma ignimbrites and ashes (Schildgen, 2008; Ouimet et al., 2008). However, if the convexity is a bedrock knickpoint and not simply a recent perturbation of the river profile, it is nonetheless small in magnitude compared to the depth of the canyon at that location (Fig. 7), and does not appear to have delimited headward propagation of major canyon incision.

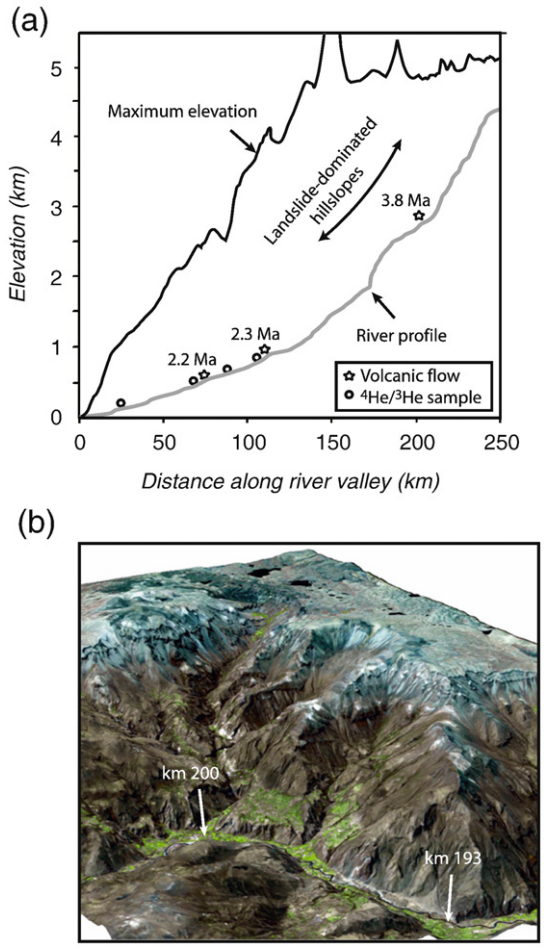

Fig. 7. a: River profile and surrounding topography. River profile extracted from 1:100,000 scale topographic maps, and surrounding topography derived from a 50-km wide swath profile of 90-m resolution SRTM digital elevation data. Locations indicated for $^{4}He/^{3}He$ samples (circles) and $^{40}Ar/^{39}Ar$ samples (stars). b: 15-m resolution ASTER image draped over a 30-m resolution ASTER DEM showing scallop-shaped landslide scarps and landslide infill from the landslide-dominated region of the upper Cotahuasi valley. Kilometer marks indicate distance along river valley from the coast and are equivalent to those shown in a.

Rather than providing a representative estimate for knickpoint propagation along the whole river profile, an alternative possibility is that our data to reveal a local slowing of the upstream propagation of incision in the middle reaches of the canyon. Such slowing may have also occurred downstream, which would mean that the start of incision (and a minimum age estimate on the start of surface uplift) may have occurred earlier than previously reported. Although our data currently do not resolve knickpoint propagation rates downstream from sample 05TS11, additional $^{4}He/^{3}He$ data from the lower reaches of the canyon may help resolve this question.

Knickpoints preserved along river profiles in northern Chile reveal slow knickpoint propagation rates that have persisted for millions of years. For example, Schlunegger et al. (2006) reported a knickpoint propagation rate of ~10 km/Ma since the late Miocene, and Hoke et al. (2007) reported a rate of 1.6 km/Ma over the past 6.4 Ma. These studies as well as ours show that knickpoint propagation rates can vary substantially both locally and among different catchments within the coastal drainages of southwest Peru and northern Chile, highlighting the complexity of river incision responses to surface uplift. Additional studies are therefore needed to help reveal details of regional incision processes that have been used as proxies for surface uplift (e.g., Gubbels et al., 1993; Kennan et al., 1997; Clark et al., 2005; Barke and Lamb, 2006; Schildgen et al., 2007, 2009a; Hoke et al., 2007).

7. Conclusions

Apatite $^{4}He/^{3}He$ thermochronometry of four samples from the Cotahuasi–Ocoña canyon system reveals an increase in cooling rate at 13–8 Ma associated with canyon incision in response to regional surface uplift. The independently derived cooling paths of these four samples are in excellent agreement with cooling paths derived from a three-dimensional thermal model interpolation to a large set of geographically distributed conventional apatite (U–Th)/He ages. Both data sets and interpretive methods yield similar estimates for the timing of incision onset, which limits the timing of Peruvian surface uplift to be prior to 8 Ma. These results highlight two aspects of $^{4}He/^{3}He$ thermochronometry: the ability to constrain continuous low-temperature cooling histories from individual samples without recourse to thermal model spatial interpolation, and efficacy for testing models of fluvial incision even if canyon depths do not exceed the pre-incision position of the PRZ.

Understanding details of the fluvial response to surface uplift is necessary for canyon incision to be an effective proxy for surface uplift. Because $^{4}He/^{3}He$ thermochronometry permits independent reconstruction of the cooling paths of multiple samples, it is also valuable in exploring the geographic and temporal pattern of exhumation. In this study, cooling paths of two samples from the upper canyon differ more than permitted by thermal models driven by simultaneous incision at both sites, requiring that canyon incision occurred later at the upstream site. This indicates that at least a portion of the canyon system developed by headward knickpoint propagation. The apparent rate of knickpoint propagation (~6 to 12 km/Ma) between these two sites may indicate that asynchronous incision occurred along the entire drainage system. Although geologic and geomorphic evidence upstream from the two sites support more rapid propagation of the incision signal upstream from the sites, we have not yet tested whether the region downstream from the sites was characterized by slow knickpoint propagation. A more extensive set of samples analyzed with $^{4}He/^{3}He$ thermochronometry would allow us to directly test whether or

not incision was time-transgressive across a much greater length of the canyon.

Acknowledgments

We thank Todd Ehlers for providing a modified version of the Pecube program that allows for extraction of *t*–*T* paths for comparison to $^4He/^3He$ data, and Ed Sobel, Dirk Sherler, Alex Rohrmann, Paolo Ballato, and Angela Landgraf for discussions. Comments from two anonymous reviews helped to improve the manuscript. We acknowledge financial support from NSF MRI grant EAR-0618219 (to D.L.S.), NSF Petrology and Geochemistry grant EAR-0738474 (to D.L.S.), NSF Tectonics grant EAR-0836203 (to K.V. Hodges and K.X. Whipple), the Ann and Gordon Getty Foundation, and the DFG-Leibnitz Center for Surface Processes and Climate Studies at the University of Potsdam.

Appendix A. Supplementary data

Supplementary data associated with this article can be found, in the online version, at doi:10.1016/j.epsl.2010.03.009.

References

Alpers, C.N., Brimhall, G.H., 1988. Middle Miocene climatic-change in the Atacama Desert, northern Chile—evidence from supergene mineralization at La-Escondida. Geol. Soc. Am. Bull. 100, 1640–1656.

Benfield, A.E., 1949. The effect of uplift and denudation on underground temperatures. J. Appl. Phys. 20, 66–70.

Barke, R., Lamb, S., 2006. Late Cenozoic uplift of the Eastern Cordillera, Bolivian Andes. Earth Planet. Sci. Lett. 249, 350–367.

Bookhagen, B., Strecker, M.R., 2008. Orographic barriers, high-resolution TRMM rainfall, and relief variations along the eastern Andes. Geophys. Res. Lett. 35 (6), L06403. doi:10.1029/2007GL032011.

Braun, J., 2002. Quantifying the effect of recent relief changes on age-elevation relationships. Earth Planet. Sci. Lett. 200, 331–343.

Braun, J., 2005. Quantitative constraints on the rate of landform evolution derived from low-temperature thermochronology. Rev. Mineral. Geochem. 58, 351–374.

Braun, J., Robert, X., 2005. Constraints on the rate of post-orogenic erosional decay from low-temperature thermochronological data: application to the Dabie Shan, China. Earth Surf. Proc. Land. 30 (9), 1203–1225.

Clark, M.K., House, M.A., Royden, L.H., Whipple, K.X., Burchfiel, B.C., Zhang, X., Tang, W., 2005. Late Cenozoic uplift of southeastern Tibet. Geology 33 (6), 525–528.

Colgan, J.P., Shuster, D.L., Reiners, P.W., 2008. Two-phase Neogene extension in the northwestern Basin and Range recorded in a single thermochronology sample. Geology 36 (8), 631–634.

Ehlers, T.A., Farley, K.A., 2003. Apatite (U–Th)/He thermochronometry: methods and applications to problems in tectonics and surface processes. Earth Planet. Sci. Lett. Front. 206, 1–14.

Ehlers, T.A., Poulsen, C.J., 2009. Large paleoclimate influence on interpretation of Andean Plateau paleoaltimetry. Earth Planet. Sci. Lett. 281, 238–248.

Farley, K.A., 2000. Helium diffusion from apatite: general behavior as illustrated by Durango fluorapatite. J. Geophys. Res. Solid Earth 105 (B2), 2903–2914.

Flowers, R.M., Ketcham, R.A., Shuster, D.L., Farley, K.A., 2009. Apatite (U–Th)/He thermochronology using a radiation damage accumulation and annealing model. Geochim. Cosmochim. Acta 73 (8), 2347–2365.

Gubbels, T.L., Isacks, B.L., Farrar, E., 1993. High-level surfaces, plateau uplift, and foreland development, Bolivian central Andes. Geology 21, 695–698.

Herman, F., Braun, J., Dunlap, W.J., 2007. Tectonomorphic scenarios in the Southern Alps of New Zealand. J. Geophys. Res. Solid Earth 112 (B4).

Hoke, G.D., Isacks, B.L., Jordan, T.E., Blanco, N., Tomlinson, A.J., Ramezani, J., 2007. Geomorphic evidence for post-10 Ma uplift of the western flank of the central Andes 18 degrees 30′–22 degrees S. Tectonics 26 (5), TC5021. doi:10.1029/2006TC002082.

Houston, J., Hartley, A.J., 2003. The central Andean west-slope rainshadow and its potential contribution to the origin of hyper-aridity in the Atacama desert. Int. J. Climatol. 23, 1453–1464.

Huntington, K.W., Ehlers, T.A., Hodges, K.V., Whipp Jr, D.M., 2007. Topography, exhumation pathway, age uncertainties, and the interpretation of thermochronometer ages. Tectonics 26, TC4012. doi:10.1029/2007TC002108.

Instituto Geológico Minero y Metalúrgico (INGEMMET), 2001. Mapa Geológico del cuadrángulo de Caravelí, Ocoña, La Yesera, y Chuquibamba. Instituto Geológico Minero y Metalúrgico. Scale 1:100,000.

Isacks, B.L., 1988. Uplift of the central Andean Plateau and bending of the Bolivian Orocline. J. Geophys. Res. 93 (B4), 3211–3231.

Kennan, L., Lamb, S., Hoke, L., 1997. High-altitude paleosurfaces in the Bolivian Andes: evidence for late Cenozoic surface uplift. In: Widdowson, M. (Ed.), Paleosurfaces: Recognition, Reconstruction and Paleoenvironmental Interpretation. Geological Society Special Publication, vol. 120. Geological Society of London, pp. 307–324.

Ketcham, R.A., 2005. Forward and inverse modeling of low-temperature thermochronology data. Rev. Mineral. Geochem. 58, 275–314.

Kirby, E., Whipple, K., 2001. Quantifying differential rock-uplift rates via stream profile analysis. Geology 29, 415–418.

Lees, C.H., 1910. On the shape of the isogeotherms under mountain ranges in radioactive districts. Proc. Roy. Soc. London 83, 339–346.

Lenters, J.D., Cook, K.H., 1995. Simulation and diagnosis of the regional summertime precipitation climatology of South America. J. Climate 8, 2988–3005.

Lenters, J.D., Cook, K.H., 1997. On the origin of the Bolivian high and related circulation features of the South American climate. J. Atmos. Sci. 54, 656–677.

Mancktelow, N.S., Grasemann, B., 1997. Time-dependent effects of heat advection and topography on cooling histories during erosion. Tectonophysics 270, 167–195.

Miller, K.G., Kominz, M.A., Browning, J.V., Wright, J.D., Mountain, G.S., Katz, M.E., Sugarman, P.J., Cramer, B.S., Christie-Blick, N., Pekar, S.F., 2005. The Phanerozoic record of global sea-level change. Science 310 (5752), 1293–1298. doi:10.1126/science.1116412.

Ouimet, W.B., Whipple, K.X., Crosby, B.T., Johnson, J.P., Schildgen, T.F., 2008. Epigenetic gorges in fluvial landscapes. Earth Surf. Proc. Land. 33 (13), 1993–2009.

Rech, J.A., Currie, B.S., Michalski, G., Cowan, A.M., 2006. Neogene climate change and uplift in the Atacama Desert, Chile. Geology 34, 761–764. doi:10.1130/G22444.1.

Reiners, P.W., Farley, K.A., 2001. Influence of crystal size on apatite (U–Th)/He thermochronology: an example from the Bighorn Mountains, Wyoming. Earth Planet. Sci. Lett. 188 (3–4), 413–420.

Roperch, P., Sempere, T., Macedo, O., Arriagada, C., Fornari, M., Tapia, C., García, M., Laj, C., 2006. Counterclockwise rotation of late Eocene–Oligocene fore-arc deposits in southern Peru and its significance for oroclinal bending in the central Andes. Tectonics 25.

Rosenbloom, N.A., Anderson, R.S., 1994. Evolution of the marine terraced landscape, Santa Cruz, California. J. Geophys. Res. 99, 14,013–14,030.

Schildgen, T. F., 2008. Surface uplift, fluvial incision, and geodynamics of plateau evolution, from the western margin of the Central Andean plateau. Ph.D. Thesis, Massachusetts Institute of Technology, Cambridge, Massachusetts, 154 p.

Schildgen, T.F., Hodges, K.V., Whipple, K.X., Reiners, P.W., Pringle, M.S., 2007. Uplift of the western margin of the Andean plateau revealed from canyon incision history, southern Peru. Geology 35 (6), 523–526.

Schildgen, T.F., Ehlers, T.A., Whipp Jr., D.M., van Soest, M.C., Whipple, K.X., Hodges, K.V., 2009a. Quantifying canyon incision and Andean Plateau surface uplift, southwest Peru: a thermochronometer and numerical modeling approach. J. Geophys. Res. Earth Surf. 114, F04014. doi:10.1029/2009JF001305.

Schildgen, T.F., Hodges, K.V., Whipple, K.X., Pringle, M.S., van Soest, M., Cornell, K.M., 2009b. Late Cenozoic structural and tectonic development of the western margin of the Central Andean Plateau in southwest Peru. Tectonics 28, TC4007. doi:10.1029/2008TC002403.

Schlunegger, F., Zeilinger, G., Kounov, A., Kober, F., Hüsser, B., 2006. Scale of relief growth in the forearc of the Andes of northern Chile (Arica latitude, 18 degrees S). Terra Nova 18 (3), 217–223.

Seeber, L., Gornitz, V., 1983. River profiles along the Himalayan arc as indicators of active tectonics. Tectonophysics 92, 335–367.

Seidl, M., Dietrich, W.E., Kirchner, J.W., 1994. Longitudinal profile development into bedrock: an analysis of Hawaiian channels. J. Geol. 102, 457–474.

Seidl, M.A., Weissel, J.K., Pratson, L.F., 1996. The kinematics of escarpment retreat across the rifted continental margin of SE Australia. Basin Res. 12, 301–316.

Sempere, T., Fornari, M., Acosta, J., Flores, A., Jacay, J., Peña, D., Roperch, P., Taipe, E., 2004. Estratigrafía, geochronología, paleogeografía y paleotectónica de los dépositos de antearco del sur del Perú. XII Congreso Peruano de Geología, Geología del Perú, Lima.

Shuster, D.L., Farley, K.A., 2004. He-4/He-3 thermochronometry. Earth Planet. Sci. Lett. 217 (1–2), 1–17.

Shuster, D.L., Farley, K.A., Sisterson, J.M., Burnett, D.S., 2004. Quantifying the diffusion kinetics and spatial distributions of radiogenic He-4 in minerals containing proton-induced He-3. Earth Planet. Sci. Lett. 217 (1–2), 19–32.

Shuster, D.L., Ehlers, T.A., Rusmore, M.R., Farley, K.A., 2005. Rapid glacial erosion at 18 Ma revealed by $^4He/^3He$ thermochronometry. Science 310, 1668–1670.

Shuster, D.L., Farley, K.A., 2005. $^4He/^3He$ thermochronometry: theory, practice, and potential complications. In: Reiners, P., Ehlers, T. (Eds.), Reviews in Mineralogy and Geochemistry: Low-Temperature Thermochronology: Techniques, Interpretations, and Applications, vol. 58, pp. 181–203.

Shuster, D.L., Flowers, R.M., Farley, K.A., 2006. The influence of natural radiation damage on helium diffusion kinetics in apatite. Earth Planet. Sci. Lett. 249 (3–4), 148–161.

Sillitoe, R.H., McKee, E.H., 1996. Age of supergene oxidation and enrichment in the Chilean porphyry copper province. Econ. Geol. Bull. Soc. 91, 164–179.

Snyder, N.P., Whipple, K.X., Tucker, G.E., Merritts, D.J., 2000. Landscape response to tectonic forcing: digital elevation model analysis of stream profiles in the Mendocino triple junction region, northern California. Geol. Soc. Am. Bull. 112, 1250–1263. doi:10.1130/0016-7606.

Strecker, M.R., Alonso, R.N., Bookhagen, B., Carrapa, B., Hilley, G.E., Sobel, E.R., Trauth, M.H., 2007. Tectonics and climate of the southern Central Andes. Annu. Rev. Earth Planet. Sci. 35, 747–787.

Stüwe, K., White, L., Brown, R., 1994. The influence of eroding topography on steady-state isotherms. Application to fission-track analysis. Earth Planet. Sci. Lett. 124, 63–74.

Thouret, J.-C., Wörner, G., Gunnell, Y., Singer, B., Zhang, X., Souriot, T., 2007. Geochronologic and stratigraphic constraints on canyon incision and Miocene uplift of the Central Andes in Peru. Earth Planet. Sci. Lett. 263, 151–166.

Whipp Jr., D.M., Ehlers, T.A., Blythe, A.E., Huntington, K.W., Hodges, K.V., Burbank, D.W., 2007. Plio-Quaternary exhumation history of the central Nepalese Himalaya: 2. thermokinematic and thermochronometer age prediction model. Tectonics 26 (3), TC3003. doi:10.1029/2006TC001991.

Whipple, K.X., Tucker, G.E., 1999. Dynamics of the stream-power river incision model: implications for height limits of mountain ranges, landscape response timescales, and research needs. J. Geophys. Res. 104, 17,661–17,674.

Whipple, K.X., Tucker, G.E., 2002. Implications of sediment-flux-dependent river incision models for landscape evolution. J. Geophys. Res. 107 (B2). doi:10.1029/2000JB000044.

Wobus, C.W., Hodges, K.V., Whipple, K.X., 2003. Has focused denudation sustained active thrusting at the Himalayan topographic front? Geology 31, 861–864. doi:10.1130/G19730.1.

Wobus, C.W., Whipple, K.X., Kirby, E., Snyder, N.P., Johnson, J., Spyropolou, K., Crosby, B., Sheehan, D., 2006. Tectonics from topography: procedures, promise and pitfalls, in tectonics, climate and landscape evolution. In: Willett, S.D., et al. (Ed.), Special Penrose Publication, vol. 398. Geological Society of America, pp. 55–74.

Wörner, G., Uhlig, D., Kohler, I., Seyfried, H., 2002. Evolution of the West Andean Escarpment at 18°S (N. Chile) during the last 25 Ma: uplift, erosion and collapse through time. Tectonophysics 345, 183–198. doi:10.1016/S0040-1951(01)00212-8.

Zaprowski, B.J., Pazzaglia, F.J., Evenson, E.B., 2005. Climatic influences on profile concavity and river incision. J. Geophys. Res. 110, F03004. doi:10.1029/2004JF000138.